



Electrochemical cutting with inner-jet electrolyte flushing for titanium alloy (Ti-6Al-4V)

Tao Yang¹ · Yanliang Li¹ · Zhengyang Xu¹ · Yongbin Zeng¹

Received: 27 August 2020 / Accepted: 9 December 2020 / Published online: 7 January 2021
© The Author(s), under exclusive licence to Springer-Verlag London Ltd. part of Springer Nature 2021

Abstract

Titanium alloys are widely used in aerospace, weapon equipment, biomedicine, and other fields because of their excellent material properties. Thus, corresponding cutting technologies that can achieve high efficiency and high quality have become the focus of research. Electrochemical cutting is a machining method that uses linear metals (wires, rods, or tubes) as the tool cathode to dissolve and remove the local material of the anode workpiece in a two-dimensional plane. This results in high-quality ruled surface structures with no burrs, recasting layers, and micro-cracks on the machining surface. However, in the electrochemical machining of titanium alloys, the electrolysis products are mostly insoluble floccules that are easily adsorbed on the machining surface, making it difficult for conventional wire electrochemical machining to complete the cutting process. To solve this problem, the electrochemical cutting of Ti-6Al-4V by inner-jet electrolyte flushing with a tube electrode is investigated. Experiments show that the optimal trade-off between machining efficiency and machining accuracy is achieved when 5% NaNO₃ + 5% NaCl electrolyte is used. Furthermore, the method of inner-jet electrolyte flushing assisted by outer-jet electrolyte flushing can be used to wash away the electrolysis products in the slit that has been cut, thus eliminating the local corrosion phenomenon on the upper surface of the slit caused by the accumulation of electrolysis products. Finally, the optimal nozzle diameter, flow rate, and electrolyte temperature were selected, and several typical structures are machined on a 10-mm-thick Ti-6Al-4V alloy block using the 5% NaNO₃ + 5% NaCl electrolyte and outer-jet electrolyte flushing-assisted machining.

Keywords Ti-6Al-4V alloy · Electrochemical cutting · Inner-jet electrolyte flushing · Electrolyte type · Outer-jet electrolyte flushing aided

1 Introduction

Titanium alloys have many excellent properties—a low density of about 60% of ordinary steel, high specific strength, and better corrosion resistance than most stainless steels because of the thin and dense oxide layer that is easily formed on their surface. They also have a wide range of stable working temperatures, and good mechanical properties persist at high or low temperature [1, 2]. Thus, titanium alloys offer an ideal structural material for aeronautics and astronautics and are often used to manufacture the blisks, blades, casing, and other parts of aero-engines

in an attempt to reduce the weight of the engine and improve the thrust-to-weight ratio of the aircraft [3].

However, the abovementioned characteristics make it difficult for common machining methods to achieve high-efficiency, high-quality machining of titanium alloys. Due to the low elastic modulus of titanium alloys, high machining stress and serious tool loss occur during milling and turning. Moreover, the sticking phenomenon of tools can easily occur due to the high cutting temperature, further reducing the machining efficiency [4]. The high melting point and poor thermal conductivity of titanium alloys mean that high energies are required to fully vaporize and remove local material during electrical discharge machining. Thicker recasting and heat-affected layers will be produced, resulting in poor surface integrity [5, 6].

To enable high-efficiency and high-quality machining of titanium alloys, electrochemical machining (ECM) has several advantages. This method is based on the principle of electrochemical anode dissolution and involves dissolving and

✉ Yongbin Zeng
binyz@nuaa.edu.cn

¹ Jiangsu Key Laboratory of Precision and Micro-Manufacturing Technology, Nanjing University of Aeronautics and Astronautics, Nanjing 210016, China

removing the local materials in the electrolyte. During the machining process, the local material of the workpiece is removed at the form of ions, the strength and hardness limits of the material are breached, and a surface with no burrs, recast layers, or micro-cracks can be obtained. There is always a certain machining gap and the cathode does not contact the anode, so no machining stress is generated. The tool cathode can be reused because it is not dissolved and only hydrogen bubbles are generated on the surface [7, 8]. At present, ECM is widely applied in the machining of titanium alloys, achieving high machining efficiency and good machining quality [9]. For example, the blisk channel of an aero-engine has been electrochemically machined on the titanium alloy Ti60 by forming a cathode radial feed [10]. Aero-engine blades have also been electrochemically machined using a γ -TiAl alloy with cathodes made of two anti-copied tool electrodes [11]. L-shaped features were formed on Ti-6Al-4V alloy by electrochemical milling in a mixed electrolyte [12], while the groove structure of a thread has been machined on Ti-6Al-4V by electrochemical turning with a wire electrode [13].

In recent years, the electrochemical cutting of titanium alloys has become the focus of much research. It is hoped that high-quality ruled surface structure parts, such as turbine disk/blade mortise and tenon joints, can be rapidly processed using the relative feed motion of a tool electrode in the two-dimensional plane. However, it is difficult to machine titanium alloys by electrochemical cutting [14]. The electrochemical dissolution characteristics of titanium alloys mean that a thick passive film is easily generated on the machining surface during ECM, which increases the transpassive potential. Moreover, the electrolysis products are usually insoluble flocules, which are easily adsorbed on the machining surface and hinder the processing. In terms of the technological characteristics of electrochemical cutting, the machining gap is long and narrow, and the electrolysis products in the machining gap are difficult to remove quickly, which worsens the consistency of the distribution of the electric and flow fields and reduces the machining efficiency and accuracy [15]. This phenomenon becomes more significant as the thickness of the workpiece increases.

To accelerate the removal of electrolysis products and enhance the refresh rate of electrolyte in the machining gap, and thus realize high-efficiency electrochemical cutting of titanium alloys, the conventional metal-wire cathode can be replaced by a helical tool that accelerates the diffusion of electrolysis products in the machining gap through its high-speed rotational motion. At the same time, a NaCl–ethylene glycol electrolyte can be used to reduce the production of passive film in the ECM process and improve the machinability of the material. This approach has enabled a square spiral microstructure to be fabricated on 0.5-mm-thick titanium plates at a feed rate of 0.3 $\mu\text{m/s}$ [16]. Although the electrochemical cutting of titanium alloy was realized by this method, the

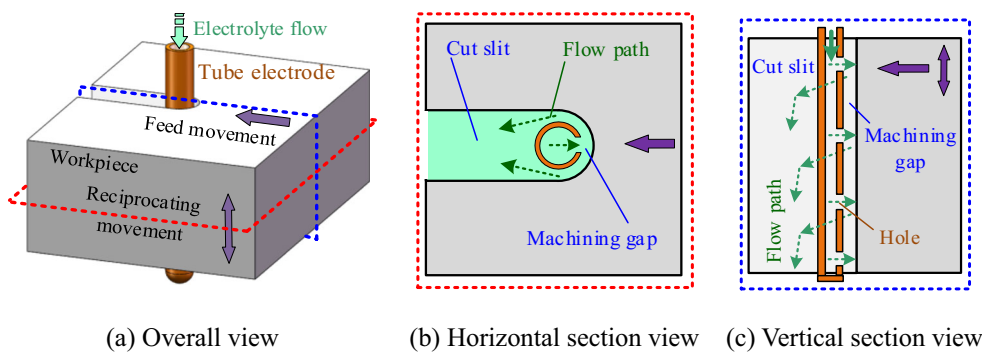
machining efficiency is low and the workpiece must be relatively thin. A method of electrochemical cutting with axial electrolyte flushing has also been proposed. A high-flow-velocity electrolyte is sprayed into the machining gap along the axial direction of a wire electrode, quickly washing away the electrolysis products, and thus accelerating the electrochemical reaction rate and improving the machining efficiency. With optimized machining parameters, a square hole structure was machined on a titanium alloy (TC1) sheet of 1.8 mm thickness at a feed rate of up to 30 $\mu\text{m/s}$ [17]. However, as the workpiece thickness increases, the flow path of the electrolyte in the machining gap becomes longer and the flow resistance increases. As a result, the flow velocity decreases greatly, which negatively affects the machining efficiency. For example, the feed rate decreases to 3 $\mu\text{m/s}$ when 10-mm-thick γ -TiAl alloys are processed by this method [18]. Moreover, the slit width varies along the direction of the slit depth, and the machining accuracy is reduced.

It is clear from the above discussion that current electrochemical cutting methods cannot achieve high-efficiency, high-accuracy machining of large-thickness ruled surface structure parts. Thus, a method is required that ensures sufficient fresh electrolyte is added to the whole machining gap in a timely manner, that the electrolysis products are quickly washed away, and that the high-efficiency and high-accuracy electrochemical cutting of relatively thick titanium alloy workpieces can be completed. This paper describes a method that enables the electrochemical cutting of Ti-6Al-4V alloy with a thickness of 10 mm using a tube electrode with an array of holes and inner-jet electrolyte flushing. The effects of different types of electrolytes on the maximum feed rate (MFR), slit width, and standard deviation are investigated and analyzed. In addition, inner-jet electrolyte flushing assisted by outer-jet electrolyte flushing is used to eliminate stray corrosion on the surface of the slit caused by the accumulation of electrolysis products in the slit. Finally, the optimal nozzle diameter, flow rate, and electrolyte temperature were selected, and several typical structures are machined on a 10-mm-thick Ti-6Al-4V alloy block using the 5% NaNO_3 + 5% NaCl electrolyte and outer-jet electrolyte flushing-assisted machining.

2 Machining principle and experimental details

Ti-6Al-4V alloy with a thickness of 10 mm was selected as the cutting object, and a metal tube with jet holes on the sidewall was selected as the tool electrode. Figure 1 shows a schematic diagram of the electrochemical cutting principle with inner-jet electrolyte flushing. The electrolyte enters through the inlet of the top end of the tube electrode, is ejected from the jet holes on the sidewall, and sprays into the machining gap along the

Fig. 1 Schematic diagram of machining principle. **a** Overall view. **b** Horizontal section view. **c** Vertical section view



radial direction of the tube electrode to participate in the electrochemical reaction. It then flows out of the machining gap from both sides of the tube electrode and enters the slit that has been cut. Finally, it flows out of the slit along the back of the tube electrode. With the flow of the electrolyte, the electrolysis products are flushed out. During the flow process, the flow stroke of the electrolyte in the machining gap area is only 1/4 of the circumference of the tube electrode cross-section. Compared with axial electrolyte flushing, the flow stroke of the electrolyte is greatly shortened and the removal efficiency of the electrolysis products is improved. In addition, the workpiece reciprocates along the axial direction of the tube electrode, which allows the electrolyte flow in each cell to fluctuate periodically and maintain a dynamic uniform distribution. The phenomenon whereby electrolyte in the area not facing the jet holes suffers from low flow velocity is eliminated, and the overall flow uniformity of the electrolyte in the machining gap is improved.

Figures 2 and 3 show the schematic diagram and photograph of the electrochemical cutting apparatus with inner-jet electrolyte flushing, respectively. The apparatus mainly includes a three-axis machine tool, electrolyte circulation system, electrical system, tube electrode, and other special fixtures. The XY axis motion of the machine tool realizes the relative feed motion between the workpiece and the tube electrode in the horizontal plane, and the Z axis motion of the

machine tool realizes the reciprocating motion of the workpiece along the axis of the tube electrode. The electrolyte circulation system includes a pump (J-ZR80/9.0, LiGao, the maximum output pressure is 9.0 MPa), filter (DZCR-400-32, DaZhang, the minimum filtering precision is 0.22 μm), temperature controller, pipeline, and electrolyte tank. The temperature controller is used to adjust and control the temperature of the electrolyte. The electrical system includes a high-frequency pulse power supply (YS9000D-4030, YiSheng, the pulse frequency is 1–100 kHz) and digital oscilloscope (DS6102, RIGOL, the frequency of sample extraction was 5 GSa/s).

Before cutting, the Ti-6Al-4V block (length 50 mm, width 40 mm) was polished with 1000 mesh sandpaper to remove the oxide layer on the surface, and ultrasonically cleaned in ethyl alcohol to remove any dirt. The tool electrode used in this study is commercial stainless steel tube that the closed end is machined by micro laser welding and the array holes is machined by micro laser drilling. The workpiece thickness was 10 mm, so a tube electrode with a hole spacing of 1 mm and hole number of 10 was selected, and the reciprocating amplitude and frequency of the workpiece were set, respectively, to 1 mm and 1.5 Hz [19, 20]. The outer diameter and inner diameter of the tube electrode were 0.7 mm and 0.4 mm, respectively, and the diameter of the jet holes was 0.2 mm. The machining parameters are presented in Table 1.

In electrochemical cutting, the MFR is often used to characterize the machining efficiency, and the slit width and standard deviation of slit width are used to characterize the machining accuracy. In this study, the feed rate of 5 $\mu\text{m/s}$ was used to cut workpiece. If the 10-mm-long slit is cut out stably (no short circuit occurs in the processing), this processing will be deemed as a success. Then, the processing is restarted at a faster feed rate with an increment of 0.5 $\mu\text{m/s}$. If there is a short circuit in the processing, this processing will be deemed as a failure. Then, the processing is restarted at a slower feed rate with a reduction of 0.5 $\mu\text{m/s}$. The MFR is defined as the fastest feed rate that can successfully cut a 10-mm-long slit. The MFR under different machining conditions was obtained by electrochemical cutting slit experiment. After the electrochemical cutting is completed, the slit sample was cleaned by

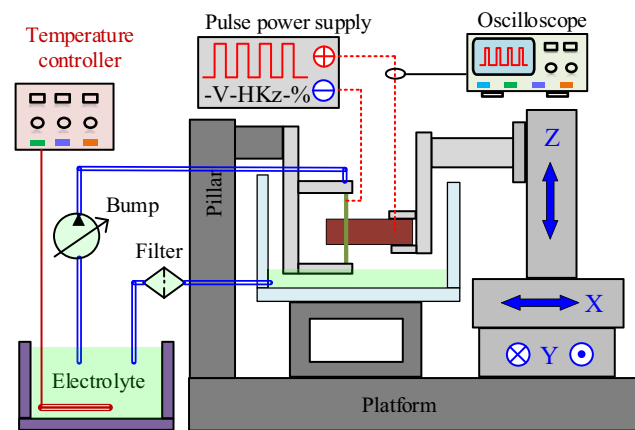
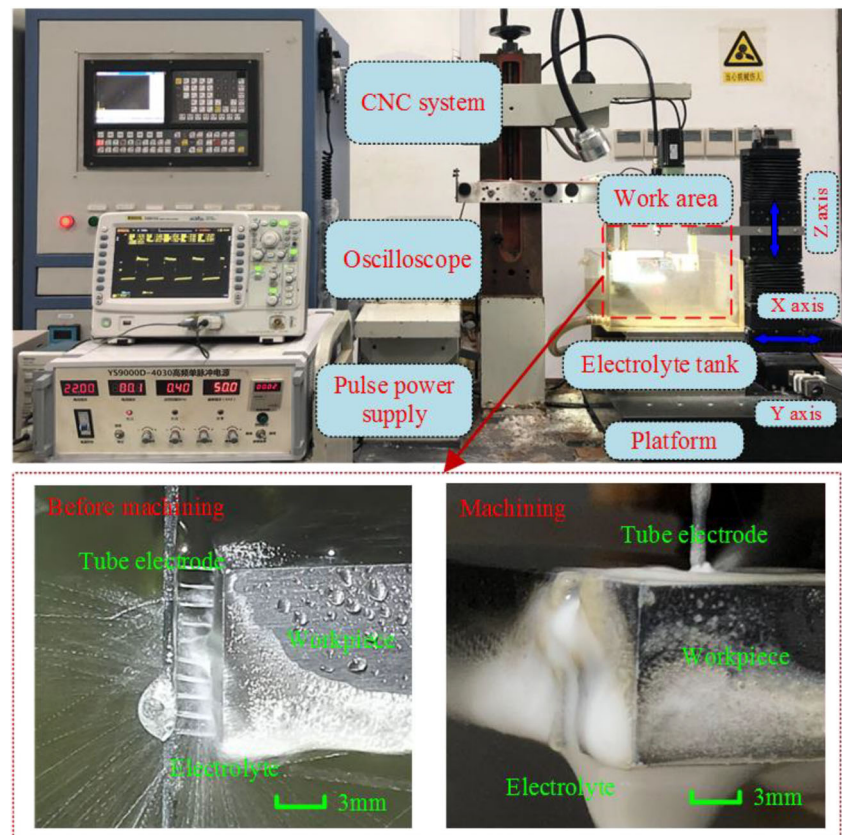


Fig. 2 Schematic diagram of the electrochemical cutting apparatus

Fig. 3 Photograph of the electrochemical cutting apparatus



ultrasonic. The morphology of the cut slit was captured by a Leica microscope (DVM5000, Germany), and the width of the cut slit was measured using an Olympus microscope (SMT7-SFA, Japan). The average and standard deviation of the slit width were calculated from ten random measurements.

3 Effect of electrolyte type

For three different electrolytes, namely 10% NaNO₃, 10% NaCl, and 5% NaNO₃ + 5% NaCl, the electrochemical cutting test was conducted at a temperature of 30 °C.

Table 1 Machining parameters

Parameters	Value
Electrical parameters	22 V (pulse voltage) 20 μs (pulse period) 8 μs (pulse width)
Electrolyte pressure	2.0 MPa
Electrolyte types	NaNO ₃ 10%wt NaCl 10%wt NaNO ₃ 5%wt + NaCl 5%wt

The process failed when 10% NaNO₃ electrolyte was used. The NO₃⁻¹ ions are passivating ions, which have a weak ability to break the passive film. The polarization curve shows that the transpassive potential of Ti-6Al-4V alloy is 9.8 V in 10% NaNO₃ electrolyte (see Fig. 4). This indicates that a high voltage is needed to break the passive film on the machining surface and cause anodic dissolution. Moreover, the main component of the passive film on the machining surface is TiO₂ when NaNO₃ electrolyte is used, as shown in Eq. (1). The hydroxide of titanium is directly generated after the electrochemical reaction, as shown in Eq. (2). As these electrolysis products are

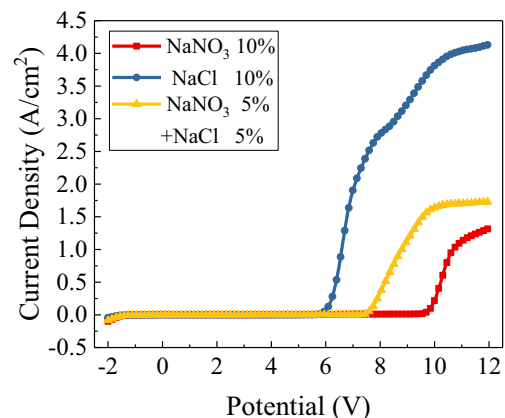
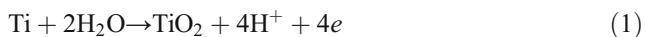


Fig. 4 Polarization curves in different types of electrolytes

adsorptive, they will adsorb on the machining surface and hinder the processing, causing the processing to fail.

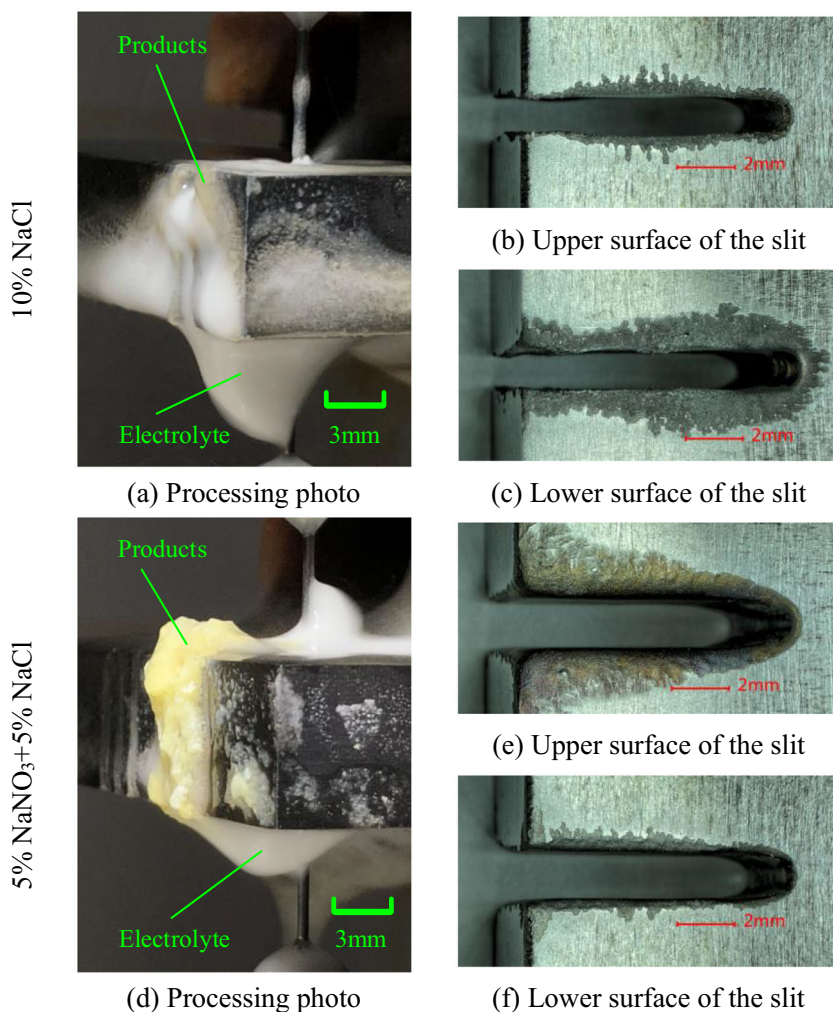


The processing proceeds smoothly when 10% NaCl electrolyte or 5% NaNO₃ + 5% NaCl electrolyte is used, allowing a slit of 10 mm length to be cut. The processing photos and machined slits are shown in Fig. 5. When 10% NaCl electrolyte is used, the Cl⁻ ions in the electrolyte are active and have a strong ability to break the passive film. The polarization curve shows that the transpassive potential of Ti-6Al-4V alloy is 5.8 V in 10% NaCl electrolyte (see Fig. 4). This indicates that a low voltage is needed to break the passive film on the machining surface and cause anodic dissolution. Moreover, the Cl⁻ ions in the electrolyte have strong reducibility and can react with the passive film on the machining surface to produce soluble chloride [21]. This chloride is flushed out of

the machining gap and slit by the fresh electrolyte ejected from the tube electrode. Finally, the soluble chloride hydrolyzes in the electrolyte to produce insoluble hydroxide [22], as shown in Eq. (3). It can be seen from Fig. 5a that, when 10% NaCl electrolyte is used, most of the waste electrolyte containing soluble chloride flows smoothly out of the slit along the back of the tube electrode and forms a drop-like shape between the tube electrode and the lower end of the slit under its own surface tension. The drop-shaped electrolyte persists and covers a large area, causing stray corrosion (see Fig. 5c) on the lower surface of the slit. However, a small amount of waste electrolyte will overflow from the upper end of the slit as the workpiece vibrates downward, causing a large amount of pitting corrosion (see Fig. 5b) on the upper surface of the slit. Finally, the electrolyte falls into the electrolyte tank under the action of gravity. In addition, a small amount of electrolysis products adhere to the wall of the slit, but there is no accumulation of electrolysis products in the slit.



Fig. 5 Processing photos and machined slit in different types of electrolytes



It can be seen from Fig. 5d that considerable electrolysis products are generated by the decrease in Cl^{-1} ions and increase in NO_3^{-1} ions in the electrolyte when 5% $\text{NaNO}_3 + 5\%$ NaCl electrolyte is used. These electrolysis products are insoluble in the electrolyte and are somewhat adhesive, which increases the flow resistance of the electrolyte and slows its flow from the machining gap to the slit. In addition, the adhesion of the electrolysis products to the slit wall makes it difficult for them to be washed away from the slit. The electrolysis products accumulate in and around the slit, hindering the flow of the electrolyte. The electrolyte that overflows from the upper end of the slit accumulates on the upper surface of the slit, making the upper surface of the workpiece susceptible to stray corrosion. With the progress of electrochemical cutting and the accumulation of electrolysis products, the range over which electrolyte overflow occurs expands, and the corrosion range on the surface of the workpiece widens. Thus, severe corrosion and removal of material occur at the incision position on the upper surface of the slit (see Fig. 5e), and the overall machining quality becomes worse. However, the stray corrosion on the lower surface of the slit is weak (see Fig. 5f). This is because the electrolyte flowing from the lower end of the slit contains a large amount of insoluble electrolysis products, and the resultant decrease in conductivity reduces the current density on the surface of the workpiece.

The variation of MFR, slit width, and standard deviation of slit width are shown in Fig. 6 for each of the different electrolyte. The highest MFR of up to 6 $\mu\text{m/s}$ is achieved with 10% NaCl electrolyte. This is because the transpassive potential is lower when 10% NaCl electrolyte is used. The Cl^{-1} ions in the electrolyte can quickly break the passive film on the machining surface and cause anodic dissolution of the workpiece at a low voltage. Moreover, the rate at which the passive film is broken is much faster than the rate at which it is generated. It can also be seen from Fig. 7 that the peak pulse current in the processing loop is 13 A. The current density on the machining surface is high and the removal of local material is fast, so the

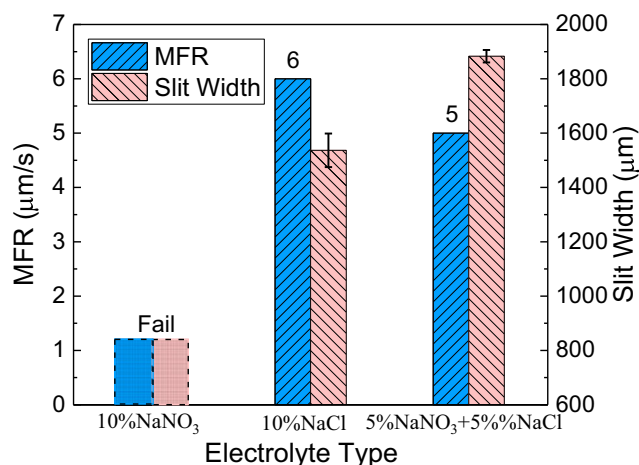


Fig. 6 Machining performance with different types of electrolytes

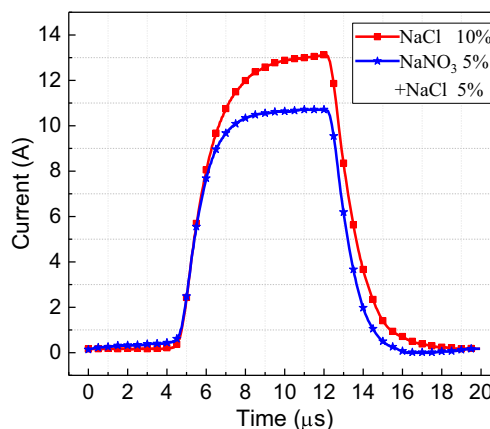


Fig. 7 Current waveform with different types of electrolytes

MFR is higher. When 5% $\text{NaNO}_3 + 5\%$ NaCl electrolyte is used, there are fewer active Cl^{-1} ions and more passivating NO_3^{-1} ions in the electrolyte, which increases the transpassive potential to 7.7 V (see Fig. 4). A higher voltage is needed to break the passive film and cause anodic dissolution. Moreover, the rate at which the passive film on the machining surface is broken is slightly faster than the generation rate. It can also be seen from Fig. 7 that the peak pulse current in the processing loop is 10.7 A. The current density on the machining surface decreases, the material removal rate slows down, and the MFR decreases to 5 $\mu\text{m/s}$.

When 10% NaCl electrolyte is used, the slit width at the MFR is smaller. This is because the faster feed rate is associated with a shorter power-on time per unit length and less material removal, and so the slit is narrower. However, the standard deviation of slit width is relatively large. This is because the activation of Cl^{-1} ions is high, and so the break rate of the passive film and the removal of materials are fast, resulting in serious stray corrosion. When 5% $\text{NaNO}_3 + 5\%$ NaCl electrolyte is used, the slit width at the MFR is larger. The decreased feed rate is associated with a longer power-on time per unit length and greater material removal, and so the slit is wider. The standard deviation of the slit width is smaller in this case. This is because there are fewer active Cl^{-1} ions and more passivating NO_3^{-1} ions in the electrolyte. The break rate of the passive film and material removal are slower, resulting in weaker stray corrosion, which improves the consistency of the slit width.

4 Inner-jet electrolyte flushing electrochemical cutting assisted by outer-jet electrolyte flushing

The results reported in the previous section indicate that the cutting efficiency is higher and the machining accuracy is lower when 10% NaCl electrolyte is used, while the optimal trade-off between machining efficiency and machining

accuracy is achieved when 5% NaNO₃ + 5% NaCl electrolyte is used for processing because this electrolyte contains the passivating ions NO₃⁻¹ and a small amount of the activate ions Cl⁻¹. To eliminate the serious stray corrosion on the upper surface of the slit caused by the accumulation of electrolysis products in and around the cut slit, this method of inner-jet electrolyte flushing electrochemical cutting was combined with outer-jet electrolyte flushing. The outer-jet electrolyte quickly flushes out the waste electrolyte that is slowly flowing from the cut slit, thus reducing the accumulation of electrolysis products in and around the cut slit, as shown in Fig. 8a. It can be seen from this figure that there is no accumulation of electrolysis products in and around the slit, and the electrolyte flows rapidly out from the slit during the cutting process. There is no serious stray corrosion on the local surface of the machined slit, as shown in Fig. 8b and c.

Figure 9 shows the variation of MFR, slit width, and standard deviation of slit width with different nozzle diameters when the flow rate of the outer-jet electrolyte is 20 L/h and the injection angle is 60°. When nozzles of different diameters are used, the MFR remains constant at the same value as that without outer-jet electrolyte flushing. This is because the outer-jet electrolyte changes the flow field in the slit, but does not change the flow field in the machining gap, and the MFR of electrochemical cutting is related to the flow field in the machining gap.

A larger nozzle diameter produces a wider slit. This is because, when a nozzle with a larger diameter is used, the injection range of the electrolyte becomes wider, and a greater corrosion area and material removal amount from the sidewall of the slit result in a wider slit. In addition, when the nozzle diameter is less than 1.9 mm, the width of the cut slit is smaller than that without outer-jet electrolyte flushing. This is because the outer-jet electrolyte quickly flushes out the waste electrolyte in the slit and restricts the flow of electrolyte to a small range, reducing the secondary electrochemical corrosion

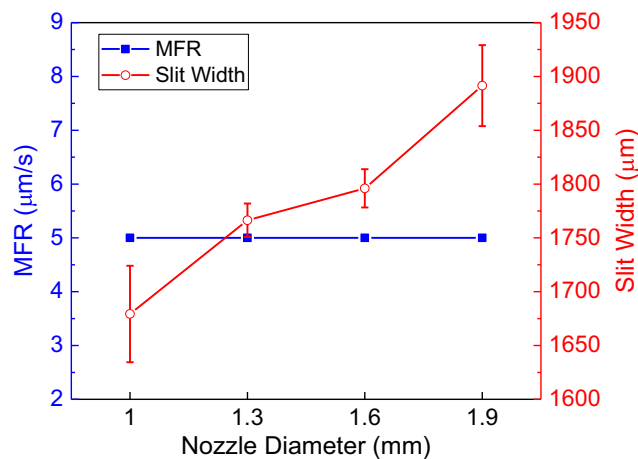
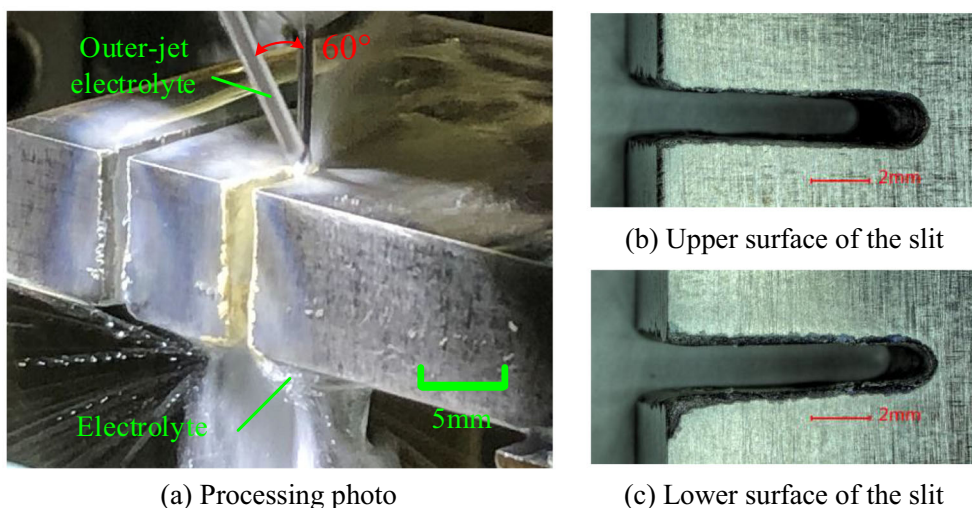


Fig. 9 Machining performance using nozzles of different diameters

caused by the waste electrolyte in the slit. When a 1.9-mm-diameter nozzle is used, the injection range of the outer-jet electrolyte is too wide and the secondary electrochemical corrosion area on the sidewall of the slit is too large, so the cut slit becomes wider.

When the nozzle has a diameter greater than 1 mm, the standard deviation of slit width gradually increases with the nozzle diameter. This is because a larger nozzle diameter widens the injection range of the outer-jet electrolyte. Moreover, the injection velocity is reduced because the flow rate is fixed, and so the binding effect of electrolyte in the slit decreases and the stray corrosion on the sidewall increases. However, when the nozzle has a diameter of 1 mm, the diameter of the electrolyte beam ejected from the smaller hole is far less than the width of the cut slit and the injection range is small, so the waste electrolyte cannot be completely flushed out from the machining gap. The electrolyte flow velocity is high in the area sprayed by the outer-jet electrolyte, while the electrolyte flow velocity is low in the area not sprayed by the outer-jet electrolyte. The flow field consistency of the

Fig. 8 Machining assisted by outer-jet electrolyte flushing. a Processing photo. b Upper surface of the slit. c Lower surface of the slit



electrolyte over the whole slit is poor, which increases the standard deviation of the slit width.

Figure 10 shows the variation of MFR, slit width, and standard deviation of slit width with outer-jet electrolyte flow rate when the nozzle diameter is 1.3 mm and the injection angle is 60° . The outer-jet electrolyte is sprayed into the slit that has been cut, and little of it is sprayed into the machining gap, which has a very weak influence on the flow field in the machining gap. Therefore, the MFR does not change with the change of flow rate. However, the slit width gradually increases with the change of flow rate. This is because, as the flow rate of the outer-jet electrolyte increases, the flow velocity of the outer-jet electrolyte sprayed into the slit will be higher, and the adhesive electrolysis products will be washed away more quickly. As a result, the conductivity of electrolyte in the slit is relatively high, the material removal amount of the slit sidewall increases, and the slit widens. When the flow rate of the outer-jet electrolyte is no more than 20 L/h, the standard deviation of slit width decreases with the flow rate increase. This is because the increase in outer-jet electrolyte flow rate accelerates the flow velocity of the electrolyte in the slit and promotes the removal of adhesive electrolysis products. The better the consistency of the electric field distribution in the slit, the more uniform the material removal of the slit sidewall, and the smaller the standard deviation of the slit width. When the flow rate of outer-jet electrolyte is greater than 20 L/h, with the increase of the electrolyte flow rate, the more serious rebound phenomenon caused by the electrolyte sprayed on the slit sidewall and the tube electrode. The consistency of the flow field in the slit will become worse, the material removal of the slit sidewall is not uniform, and the standard deviation of the slit width will increase.

Figure 11 shows the variation of MFR, slit width, and standard deviation of slit width with electrolyte temperature when the nozzle diameter is 1.3 mm and the outer-jet

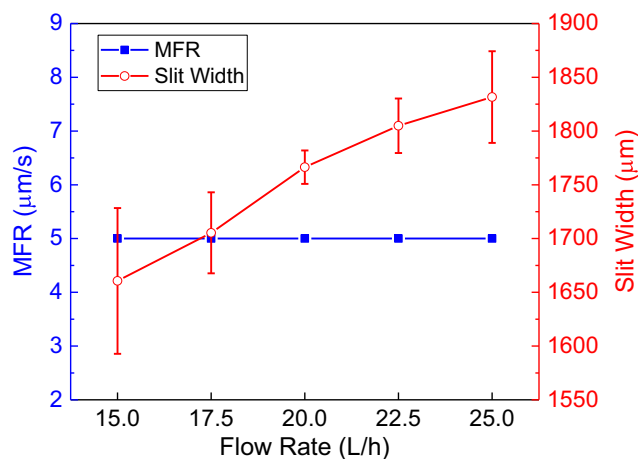


Fig. 10 Machining performance with different flow rate of the outer-jet electrolyte

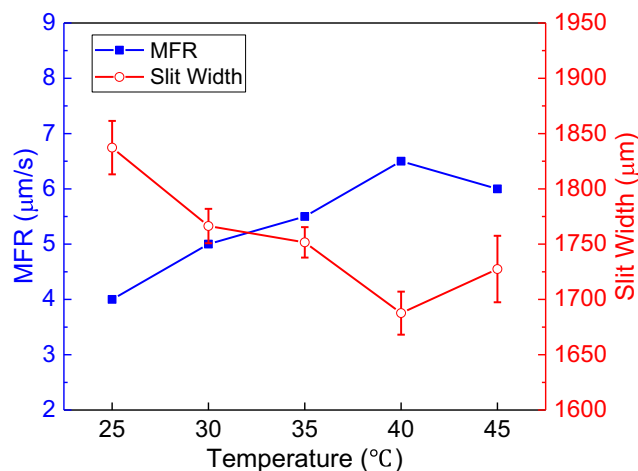
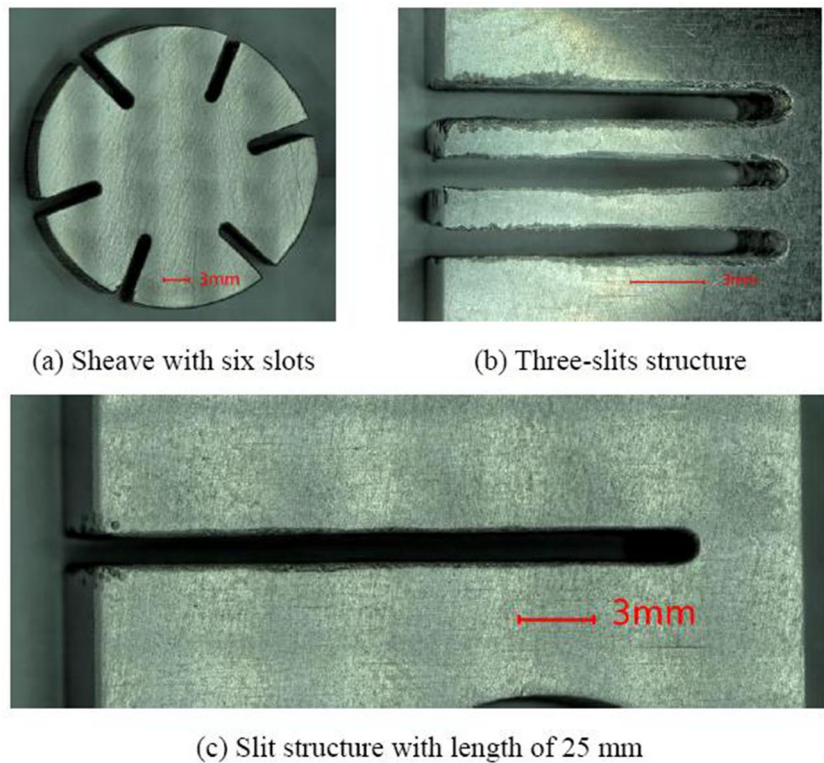


Fig. 11 Machining performance with different electrolyte temperature

electrolyte flow rate is 20 L/h. When the electrolyte temperature is lower than 40°C , the MFR gradually increases with the rise of the electrolyte temperature. This is because the increase of electrolyte temperature can enhance the activation of Cl^- ion and improve the break ability of Cl^- ion to the passive film on the machining surface. At the same time, the increase of electrolyte temperature speeds up the movement of anion and cation in the electrolyte and improves the material removal rate. Moreover, the corrosion and removal of the workpiece material is more uniform, the consistency of the slit width increases. Therefore, the standard deviation of slit width decreases with the increase of electrolyte temperature. In addition, the slit width decreases due to faster feed rate. However, the MFR decreases when the electrolyte temperature is 45°C , compared with the electrolyte temperature of 40°C . This is because when the electrolyte temperature is too high, more bubbles and electrolysis products are produced, which affects the current density distribution in the machining gap and slows down the electrochemical reaction rate. At the same time, the consistency of material removal is reduced and the standard deviation of the slit width increases. In addition, the slit width increases due to slower feed rate.

Using the experimental process described in this section, the optimal machining parameters were selected: the nozzle diameter was 1.3 mm, the flow rate of outer-jet electrolyte was 20 L/h, and electrolyte temperature was 40°C . Several typical structures were machined on a 10-mm-thick Ti-6Al-4V alloy block using the 5% NaNO_3 + 5% NaCl electrolyte and outer-jet electrolyte flushing-assisted machining. A sheave with six slots was machined at the feed rate of $5\ \mu\text{m/s}$, with an average slot width of 1.761 mm and a standard deviation of $39.3\ \mu\text{m}$, as shown in Fig. 12a. A three-slit structure and a 25-mm-long slit structure were machined at the feed rate of $6.5\ \mu\text{m/s}$, with an average slit width of 1.712 mm and a standard deviation of $25.3\ \mu\text{m}$, as shown in Fig. 12b and c.

Fig. 12 Machined structure samples of 10-mm-thick Ti-6Al-4V alloy. **a** Sheave with six slots. **b** Three-slit structure. **c** Slit structure with length of 25 mm



5 Conclusion

With the aim of enhancing the efficiency and accuracy of the electrochemical cutting of large-thickness titanium alloy workpieces, an experimental study was carried out using 10-mm-thick Ti-6Al-4V alloy samples and inner-jet electrolyte flushing with a tube electrode. The effects of different electrolyte types and outer-jet electrolyte flushing on the machining efficiency and machining accuracy were investigated. The conclusions are as follows:

- (1) The use of 5% NaNO₃ + 5% NaCl electrolyte results in a better trade-off of machining efficiency and machining accuracy than with the other electrolytes because of the decrease in Cl⁻ ions and the increase in NO₃⁻ ions. However, a large number of insoluble electrolysis products are generated, and these accumulate in and around the slit. This hinders the flow of electrolyte, causes serious stray corrosion on the upper surface of the slit, and reduces the cutting quality.
- (2) The outer-jet electrolyte quickly flushes out the slow-flowing waste electrolyte in the cut slit, which reduces the accumulation of electrolysis products in and around the slit and eliminates the serious stray corrosion on the upper surface of the slit.
- (3) The flushing of the outer-jet electrolyte has no effect on the machining efficiency, but does influence the machining accuracy. The slit width and standard

deviation of slit width can be reduced by selecting appropriate parameters of outer-jet electrolyte flushing in the case of inner-jet electrolyte flushing electrochemical cutting assisted by outer-jet flushing.

- (4) Selecting appropriate electrolyte temperature can improve the machining efficiency and machining accuracy.
- (5) Several typical structures were machined on a 10-mm-thick Ti-6Al-4V alloy block using the 5% NaNO₃ + 5% NaCl electrolyte and outer-jet electrolyte flushing assisted machining.

Authors' contributions Tao Yang conceived of the study, designed the study, and collected the data. All authors analyzed the data and were involved in writing the manuscript.

Funding This work was supported by the National Natural Science Foundation of China (91960204), the Aeronautical Science Foundation of China (201907052002), the National Natural Science Foundation of China for Creative Research Groups (51921003), and the Postgraduate Research & Practice Innovation Program of Jiangsu Province (KYCX19_0167).

Data availability All data generated or analyzed during this study are included in this article.

Compliance with ethical standards

Conflict of interest The authors declare that they have no conflict of interest.

Ethical approval The article follows the guidelines of the Committee on Publication Ethics (COPE) and involves no studies on human or animal subjects.

Consent to participate Not applicable.

Consent to publish Not applicable.

References

- Boyer RR (2010) Attributes, characteristics, and applications of titanium and its alloys. *JOM* 62:21–24. <https://doi.org/10.1007/s11837-010-0071-1>
- Kaur M, Singh K (2019) Review on titanium and titanium-based alloys as biomaterials for orthopaedic applications. *Mater Sci Eng C* 102:844–862. <https://doi.org/10.1016/j.msec.2019.04.064>
- Klocke F, Klink A, Veselovac D, Aspinwall DK, Soo SL, Schmidt M, Schilp J, Levy G, Kruth JP (2014) Turbomachinery component manufacture by application of electrochemical, electro-physical and photonic processes. *CIRP Ann - Manuf Technol* 63:703–726. <https://doi.org/10.1016/j.cirp.2014.05.004>
- Pramanik A (2014) Problems and solutions in machining of titanium alloys. *Int J Adv Manuf Technol* 70:919–928. <https://doi.org/10.1007/s00170-013-5326-x>
- Aspinwall DK, Soo SL, Berrisford AE, Walder G (2008) Workpiece surface roughness and integrity after WEDM of Ti-6Al-4V and Inconel 718 using minimum damage generator technology. *CIRP Ann - Manuf Technol* 57:187–190. <https://doi.org/10.1016/j.cirp.2008.03.054>
- Klocke F, Welling D, Dieckmann J (2011) Comparison of grinding and wire EDM concerning fatigue strength and surface integrity of machined Ti6Al4V components. *Procedia Eng* 19:184–189. <https://doi.org/10.1016/j.proeng.2011.11.099>
- Rajurkar KP, Zhu D, McGeough JA, Kozak J, Silva D (1999) New developments in electro-chemical machining. *CIRP Ann - Manuf Technol* 48:567–579. [https://doi.org/10.1016/S0007-8506\(07\)63235-1](https://doi.org/10.1016/S0007-8506(07)63235-1)
- Rajurkar K, Sundaram MM, Malshe AP (2013) Review of electrochemical and electrodischarge machining. *Procedia CIRP* 6:13–26. <https://doi.org/10.1016/j.procir.2013.03.002>
- Xu ZY, Wang YD (2019) Electrochemical machining of complex components of aero-engines: developments, trends, and technological advances. *Chinese J Aeronaut*. <https://doi.org/10.1016/j.cja.2019.09.016>
- Xu ZY, Chen XZ, Zhou ZS, Qin P, Zhu D (2016) Electrochemical machining of high-temperature titanium alloy Ti60. *Procedia CIRP* 42:125–130. <https://doi.org/10.1016/j.procir.2016.02.206>
- Liu J, Wang H, Zhu D (2018) Electrochemical machining of γ -TiAl intermetallic blades by using the stainless steel anti-copied tool electrodes. *Procedia CIRP* 68:757–761. <https://doi.org/10.1016/j.procir.2017.12.133>
- Mishra K, Dey D, Sarkar BR, Bhattacharyya B (2017) Experimental investigation into electrochemical milling of Ti6Al4V. *J Manuf Process* 29:113–123. <https://doi.org/10.1016/j.jmapro.2017.07.014>
- Sharma V, Patel DS, Jain V, Tyagi A (2018) Wire electrochemical threading: a technique for fabricating macro/micro thread profiles. *J Electrochem Soc* 165:E397–E405. <https://doi.org/10.1149/2.1181809jes>
- Zhu D, Wang K, Qu NS (2007) Micro wire electrochemical cutting by using in situ fabricated wire electrode. *CIRP Ann - Manuf Technol* 56:241–244. <https://doi.org/10.1016/j.cirp.2007.05.057>
- Gao CP, Qu NS (2019) Wire electrochemical micromachining of high-aspect ratio microstructures on stainless steel 304 with 270- μ m thickness. *Int J Adv Manuf Technol* 100:263–272. <https://doi.org/10.1007/s00170-018-2725-z>
- Yu N, Fang XL, Meng LC, Zeng Y, Zhu D (2018) Electrochemical micromachining of titanium microstructures in an NaCl–ethylene glycol electrolyte. *J Appl Electrochem* 48:263–273. <https://doi.org/10.1007/s10800-018-1145-y>
- Qu NS, Fang XL, Li W, Zeng Y, Zhu D (2013) Wire electrochemical machining with axial electrolyte flushing for titanium alloy. *Chinese J Aeronaut* 26:224–229. <https://doi.org/10.1016/j.cja.2012.12.026>
- He HD, Qu NS, Zeng YB, Fang X, Yao Y (2016) Machining accuracy in pulsed wire electrochemical machining of γ -TiAl alloy. *Int J Adv Manuf Technol* 86:2353–2359. <https://doi.org/10.1007/s00170-016-8402-1>
- Yang T, Zeng YB, Hang YS (2019) Workpiece reciprocating movement aided wire electrochemical machining using a tube electrode with an array of holes. *J Mater Process Technol* 271:634–644. <https://doi.org/10.1016/j.jmatprotec.2019.04.044>
- Yang T, Zeng YB, Sang YM, Li SY (2020) Effect of structural parameters of array of holes in the tube electrode for electrochemical cutting. *Int J Adv Manuf Technol* 107:205–216. <https://doi.org/10.1007/s00170-020-05089-0>
- Mishra K, Dey D, Sarkar BR, Bhattacharyya B (2018) Modeling on volumetric material removal for fabrication of complex shapes by EC milling of Ti6Al4V. *J Electrochem Soc* 165:388–396. <https://doi.org/10.1149/2.0911809jes>
- Godlewska E, Mitoraj M, Leszczynska K (2014) Hot corrosion of Ti–46Al–8Ta (at.%) intermetallic alloy. *Corros Sci* 78:63–70. <https://doi.org/10.1016/j.corsci.2013.08.032>

Publisher's note Springer Nature remains neutral with regard to jurisdictional claims in published maps and institutional affiliations.